Check for updates

Biparametric MRI-based radiomics classifiers for the detection of prostate cancer in patients with PSA serum levels of 4~10 ng/mL

Yangbai Lu[1†], Binfei Li[2†], Hongxing Huang[1†], Qu Leng[1], Qiang Wang[1], Rui Zhong[1], Yaqiang Huang[1], Canyong Li[1], Runqiang Yuan[1*] and Yongxin Zhang[3*]

[1]Department of Urology, Zhongshan City People's Hospital, Zhongshan, Guangdong, China,
[2]Department of Anesthesiology, Zhongshan City People's Hospital, Zhongshan, Guangdong, China,
[3]Department of Magnetic Resonance Imaging, Zhongshan City People's Hospital, Zhongshan, Guangdong, China

Purpose: To investigate the predictive performance of the combined model by integrating clinical variables and radiomic features for the accurate detection of prostate cancer (PCa) in patients with prostate-specific antigen (PSA) serum levels of 4-10 ng/mL.

Methods: A retrospective study of 136 males (mean age, 67.3 ± 8.4 years) with Prostate Imaging-Reporting and Data System (PI-RADS) v2.1 category $\leq$3 lesions and PSA serum levels of 4-10 ng/mL were performed. All patients underwent multiparametric MRI at 3.0T and transrectal ultrasound-guided systematic prostate biopsy in their clinical workup. Radiomic features were extracted from axial T2-weighted images (T2WI) and apparent diffusion coefficient (ADC) maps of each patient using PyRadiomics. Pearson correlation coefficient (PCC) and recursive feature elimination (RFE) were implemented to identify the most significant radiomic features. Independent clinic-radiological factors were identified *via* univariate and multivariate regression analyses. Seven machine-learning algorithms were compared to construct a single-layered radiomic score (ie, radscore) and multivariate regression analysis was applied to construct the fusion radscore. Finally, the radiomic nomogram was further developed by integrating useful clinic-radiological factors and fusion radscore using multivariate regression analysis. The discriminative power of the nomogram was evaluated by area under the curve (AUC), DeLong test, calibration curve, decision curve analysis (DCA), and clinical impact curve (CIC).

Results: The transitional zone-specific antigen density was identified as the only independent clinic-radiological factor, which yielded an AUC of 0.592 (95% confidence interval [CI]: 0.527-0.657). The ADC radscore based on six features and Naive Bayes achieved an AUC of 0.779 (95%CI: 0.730-0.828); the

T2WI radscore based on 13 features and Support Vector Machine yielded an AUC of 0.808 (95%CI: 0.761-0.855). The fusion radscore obtained an improved AUC of 0.844 (95%CI: 0.801-0.887), which was higher than the single-layered radscores (both P<0.05). The radiomic nomogram achieved the highest value among all models (all P<0.05), with an AUC of 0.872 (95%CI: 0.835-0.909). Calibration curve showed good agreement and DCA together with CIC confirmed the clinical benefits of the radiomic nomogram.

Conclusion: The radiomic nomogram holds the potential for accurate and noninvasive identification of PCa in patients with PI-RADS ≤3 lesions and PSA of 4-10 ng/mL, which could reduce unnecessary biopsy.

Introduction

Prostate cancer (PCa) is among the most common malignancies in the male population and is a major global health problem (1). It is crucial for patients to be diagnosed with PCa as earlier as possible while reducing unnecessary biopsies. Currently, prostate-specific antigen (PSA) and multiparametric magnetic resonance imaging (mpMRI) both play essential roles in PCa screening and the selection of suitable candidates for biopsy (2, 3). However, PSA-based screening has several challenges including an increased false positive rate, the inability to detect PCa with random biopsy, multifocality in PCa, and the molecular heterogeneity of PCa (4). Around 70% of patients with PSA levels of 4-10 ng/mL, which is a diagnostic gray zone, may undergo unnecessary biopsy (5). mpMRI is a common non-invasive imaging technology applied in the detection and diagnosis of PCa, identification of aggressive disease, as a triage test before biopsy, targeting biopsy, and active surveillance of patients after a negative biopsy (6). However, mpMRI images may contain clinically valuable information related to tumor heterogeneity and biological characteristics, which may be difficult for radiologists to interpret in clinical practice (7), which calls for more advanced methods.

Radiomics is a novel tool that involves extracting quantitative features from medical images using computational algorithms such as machine learning, which can identify new biomarkers and assess the heterogeneity of the disease (8). Recently, radiomics and its combination with machine learning techniques have shown its promise in MRI-based PCa diagnosis, which was superior to Prostate Imaging-Reporting and Data System (PI-RADS) category (9–13). mpMRI protocol suggested by PI-RADS v2.0 includes T2-weighted imaging (T2WI), diffusion-weighted imaging (DWI) and the corresponding apparent-diffusion coefficient (ADC) maps, and dynamic contrast-enhanced (DCE) imaging (14). Despite several advancements in the diagnosis of PCa using mpMRI, it still suffers from relatively high cost, inconsistent image quality, moderate specificity, and inter-observer variability in result interpretation (15, 16). Some studies have shown that the incremental value of DCE imaging over the combination of T2WI and DWI in the diagnosis of PCa is modest (17–19). The PI-RADS v2.1 emphasizes that although DCE imaging is essential, its role in the determination of the PI-RADS category is secondary to that of T2-WI and DWI (20). Previous studies have shown that in those patients with PSA levels of 4-10 ng/mL, biparametric MRI (bpMRI) achieved better performance than conventional MRI and mpMRI with higher specificity in detecting PCa and reduced unnecessary biopsies (21–23). Accordingly, this study aimed to investigate the effectiveness of radiomic features extracted from bpMRI in the identification of PCa and to develop and validate a radiomic nomogram for PCa diagnosis in a subgroup of patients with PI-RADS ≤3 lesions and PSA serum levels of 4-10 ng/mL, providing a practical tool for accurate diagnosis and personalized treatment.

Materials and methods

Patients

The Institutional Review Board approved this retrospective study and the requirement for written informed consent was waived. A total of 314 consecutive patients who underwent prostate MRI examination due to elevated PSA levels in our hospital between January 2018 and December 2021 were retrospectively reviewed. The inclusion criteria were as follows:

(1) patients who received transrectal ultrasound-guided systematic prostate biopsy; (2) patients who underwent MRI scans within one week prior to biopsy; (3) patients with PI-RADS ≤3 lesions; and (4) patients with PSA serum levels of 4-10 ng/mL. The exclusion criteria were: 1) incomplete clinical data (n=56); 2) a history of previous therapy for PCa prior to MR scans, such as radiotherapy, endocrine therapy, and chemotherapy (n=45); 3) MR images with poor image quality (such as susceptibility artifact) (n=30); 4) the puncture site did not well match with the lesion location in MR images (n=47). Finally, 136 patients (mean age, 67.3 ± 8.4; range, 38-86 years) were included in this study. The patients were randomly divided into a training dataset (n=95; 34 PCa and 61 hyperplasia) and a validation dataset (n=41; 15 PCa and 26 hyperplasia). Figure 1 illustrates the patient recruitment pathway and the inclusion and exclusion criteria.

Clinical and radiological features

Baseline clinical variables were collected from the electronic medical record system, including age, total PSA (tPSA), free PSA (fPSA), and the ratio of fPSA to tPSA (fPSA/tPSA).

The length, width, and height of the entire prostate and transition zone (TZ) were measured on mpMRI by an experienced radiologist (with 11 years of experience in prostate MRI) and checked by a senior radiologist (with 20 years of experience in prostate MRI). The transverse diameter and anteroposterior diameter of the TZ, the transverse diameter

and anteroposterior diameter of the entire prostate were measured on a horizontal section. The superoinferior diameters of the TZ and the entire prostate were measured on the sagittal plane. The prostate volume (PV) was measured at the boundary of the prostate capsule, and the transitional zone volume (TZV) was measured at the boundary of the fibrous layer of the TZ. The PV and TZV were calculated using the following ellipsoid volume formula: volume (ml) = $(\pi/6) \times$ anteroposterior diameter (cm) $\times$ transverse diameter (cm) $\times$ superoinferior diameter (cm). Peripheral zone volume (PZV) = PV - TZV. Prostate-specific antigen density (PSAD) = tPSA/PV, prostate transitional zone-specific antigen density (TZ-PSAD) = tPSA/TZV, and prostate peripheral specific antigen density (PZ-PSAD) = tPSA/PZV = tPSA/PV-TZV.

MR imaging and image Interpretation

All patients were scanned on a 3.0T MR system (Achieva, Philips Medical Systems, Best, Netherlands) with a 16-channel Sense Torso XL coil. The MRI sequences included axial T1-weighted imaging, axial, coronal, and sagittal T2WI, axial DWI, pre-contrast axial fat- suppressed T1 high-resolution isotropic volume examination (THRIVE), and post-contrast axial breath-hold DCE that performed with fat-suppressed enhanced-THRIVE. The detailed acquisition parameters of routine MR sequences are shown in Table 1.

A total of 20 periods of dynamic enhanced prostate scanning were performed, with a total scanning time of 2 min. The
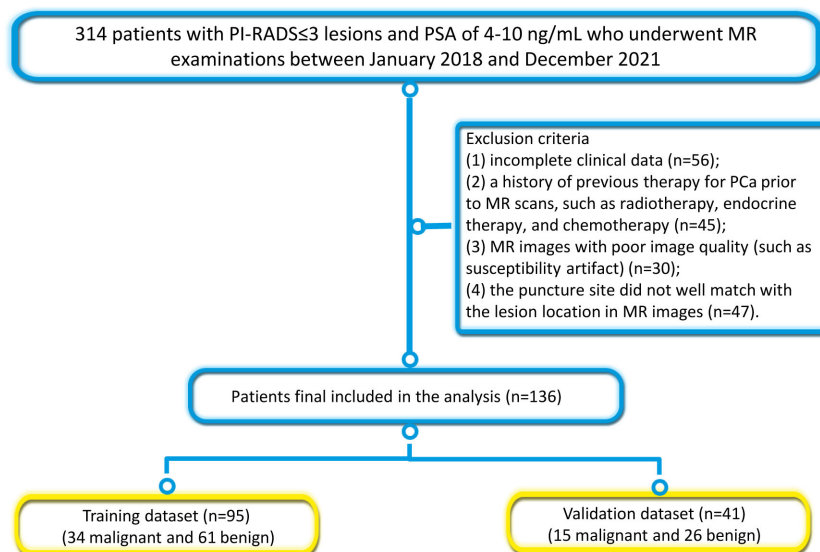

FIGURE 1
The patient recruitment pathway and the inclusion and exclusion criteria.

TABLE 1 The detailed acquisition parameters of MRI.

|	T2WI	T1WI	DWI	eTHRIVE
TR/TE (ms)	3384/120	543/8	2787/61	3.1/1.8
Flip angle (°)	90	90	90	10
Slice thickness/gap (mm)	4	4	4	4/0
Acquisition time	02:55.9	01:52.4	01:54.3	01:50.6
FOV (mm)	230× 230	230× 230	250× 250	240× 240
Matrix	250× 250	250× 250	116×114	200× 200
Reconstruction matrix	0.57×0.57	0.57×0.57	1.12×1.12	0.58×0.58
Bandwidth (Hz/pixel)	1038.6	225.6	32.2	723.4
No. of excitations	1	1	4	1
B value (s/mm^2)			0/1000	

DWI, diffusion-weighted imaging; T2WI, T2-weighted imaging; T1WI, T1-weighted imaging; e-THRIVE, enhanced T1 high-resolution isotropic volume examination; TR/TE, repetition time/echo time; FOV, field of view.

contrast agent was injected at the end of the first period. Gadodiamide (MEDRAD Healthcare, 0.2 mmol/kg body weight) was administrated *via* intravenously pumping (3.0 ml/s) followed by 20 ml of a saline flush at the same rate.

The PI-RADS v2.1 score for each case was evaluated by two radiologists (with 9 and 11 years of experience in PCa diagnosis, respectively), blinded to pathological data except for tumor location. Any discrepancy among the two observers was resolved by consulting with a third radiologist (with 20 years of experience in PCa diagnosis). The PI-RADS v2.1 scores were assessed on T2WI, DWI, and DCE-MRI images. If there were multiple lesions, the PI-RADS score was determined by the largest or most aggressive lesion.

Tumor segmentation and volume of interest construction

Figure 2 shows the workflow of this study. The manual segmentation of prostatic nodules was performed by a radiologist with 9 years of experience in PCa diagnosis using ITK-SNAP software (http://www.radiantviewer.com). The regions of interest (ROIs) were drawn by radiologists for radiomic analysis are confirmed by systematic biopsy cores. The lesions were manually outlined on each slice of the axial T2WI and ADC images separately, which covered the whole suspicious lesions and avoided the surrounding prostate capsule, peripheral blood vessels, seminal vesicle root, bleeding,

FIGURE 2
The workflow of this study.
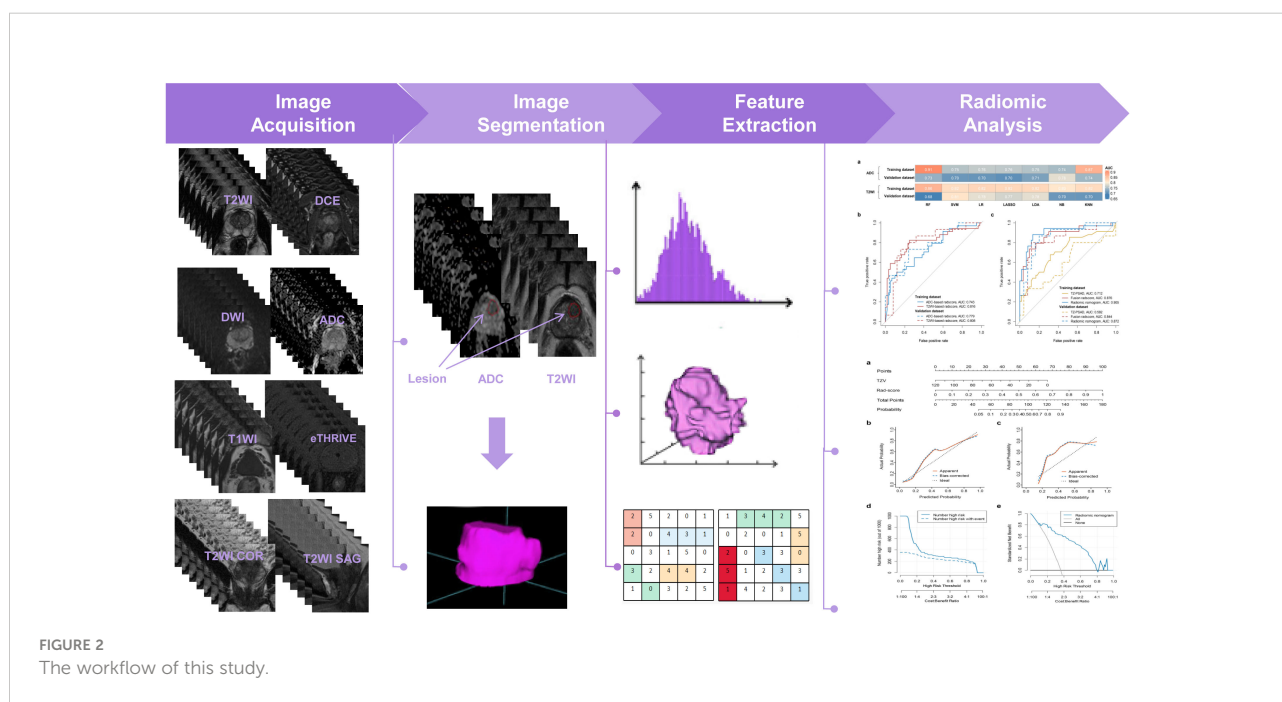
calcification, and urethra. Then, ROIs were utilized to obtain volumes of interest (VOIs). The segmentation results were independently validated by a radiologist with 11 years of experience in PCa diagnosis to reduce potential bias.

Image preprocessing

The N4 correction algorithm in the 3D Slicer (version 4.11.0; https://www.slicer.org) was used to remove the MRI offset field artifacts and reduce the inhomogeneity of the radio frequency field as well as the influence of the MR equipment itself. Then, the MRI gray value was normalized to reduce the gray difference between MRI sequences caused by different acquisition times and parameter settings, to ensure accurate and reliable radiomic analysis. Finally, the B-spline interpolation algorithm was used to resample the ROIs to a uniform size (1*1*1) for feature extraction.

Feature extraction

The calculation and extraction of radiomic features were conducted consistently with the guideline of the Image Biomarker Standardisation Initiative (24). An open source radiomic package PyRadiomics v3.0 (25) (https://pypi.org/project/pyradiomics/) was applied to extract radiomic features from the original and filtered MR images (wavelet filter and Laplacian of Gaussian filter). Among them, the Log filter sigma parameter defines the texture roughness, and we set the sigma size to 1, 3, and 5 to obtain filtered images of different textures. For wavelet filtering, the bin width is set to 10. A total of 1130 radiomic features were extracted from each MR sequence, which could be divided into four groups: i) shape-based features (n=14), ii) first-order features (n=72), iii) texture features (n=300), and iv) wavelet features (n=744). Texture features included gray-level co-occurrence matrix (GLCM), gray-level size zone matrix (GLSZM), gray-level run length matrix (GLRLM), neighboring gray tone difference matrix (NGTDM), and gray-level dependence matrix (GLDM) features.

Feature selection and radiomic score development

All radiomic features were standardized into a normal distribution with z-score normalization. A two-step feature selection process was employed by using several dimensionality reduction techniques. In the first step, we applied Pearson correlation coefficient (PCC) analysis to eliminate feature pairwise correlation and to ensure the features were independent of each other. One feature was selectively excluded from each pair with a correlation coefficient >0.99. In the second step, the remaining features were subsequently selected by the recursive feature elimination (RFE) algorithm. After that, seven machine learning classifiers were compared to build the best-performing T2WI- and ADC-based radiomic score (ie, radscore), including random forest (RF), support vector machine (SVM), logistic regression (LR), least absolute shrinkage and selection operator (LASSO), linear discriminant analysis (LDA), naive Bayes (NB), and K-nearest neighbor (KNN). Five-fold cross-validation was used for feature selection and classification algorithm optimization. The fusion radscore was obtained by linear fitting of T2WI- and ADC-based radscores using multivariate regression analysis in the training dataset.

Radiomic nomogram establishment and assessment

Clinic-radiological variables with P<0.10 in univariate logistic regression were entered into multivariate logistic regression. The stepwise regression method was used to screen the variables in the multivariate regression model. Variables with P<0.05 were considered independent factors.

A radiomic nomogram was developed by integrating significant clinic-radiological variables in univariate regression analysis and radscore *via* multivariable logistic regression. Calibration curves of the nomogram and Hosmer–Lemeshow test were used to assess the agreement between prediction and actual observation. Moreover, we performed decision curve analysis (DCA) and clinical impact curve (CIC) to evaluate the net benefit of clinical decisions.

Statistical analysis

All statistical analyses were done using R software (version 3.4.1; http://www.Rproject.org) and SPSS Statistics (version 26.0; IBM Corp., New York, USA). The distribution of continuous data was evaluated by the Kolmogorov-Smirnov test. Continuous and categorical variables were compared by t-test, Mann-Whitney U test, or Chi-square, if appropriate. The R package "glmnet" statistical software (R Foundation) was used to perform the modeling of classifiers. Other R packages were used as follows: "rms" package for multivariable logistic regression analysis and calibration curves, "pROC" package for receiver operating characteristic curve (ROC), "rmda" package for decision curve analysis (DCA), and clinical impact curve (CIC). ROC analysis was used to evaluate the classification performance of models, including area under the curve (AUC), sensitivity, specificity, and accuracy. The Delong test was used to compare the area under the curves (AUCs). P<0.05 was considered statistically significant.

Results

Patient characteristics

There were 57.4% of cases were in the TZ (benign 57.5% and malignant 57.1%). Table 2 compares the clinic-radiological characteristics of benign and malignant prostatic nodules. The results showed that PV (P<0.001), TZV (P<0.001), PSAD (P=0.010), and TZ-PSAD (P=0.001) were statistically different between benign and malignant prostatic nodules. The clinic-radiological variables between the training and validation datasets were nonsignificant (all P>0.05).

Clinical model

Univariate analysis of 11 clinic-radiological variables showed that PV (P=0.045), TZV (P=0.009), PSAD (P=0.008), and TZ-PSAD (P=0.001) were significantly associated with cancer (Table 3). The results of multivariate analysis showed that only TZ-PSAD (P=0.001) was an independent predictor of PCa (Table 3). The clinical model based on TZ-PSAD achieved an AUC of 0.712 (95%CI: 0.655-0.769) in the training dataset and 0.592 (95%CI: 0.527-0.657) in the validation dataset (Table 4).

Comparison of single-layered radscores

For the ADC sequence, 679 radiomic features were retained after PCC analysis, and six features were finally selected (Table 5). The NB-based ADC radscore yielded the highest AUC of 0.743 (95%CI: 0.690-0.796) in the training dataset and 0.779 (95%CI: 0.730-0.828) in the validation dataset (Table 4 and Figure 3). For the T2WI sequence, 681 features were retained after PCC analysis, and 13 features were finally identified (Table 5). The SVM-based T2WI radscore achieved the highest AUC of 0.816 (95%CI: 0.765-0.867) in the training dataset and 0.808 (95%CI: 0.761-0.855) in the validation dataset (Table 4 and Figure 3). Compared with the single-layered radscores, the fusion radscore obtained higher performance (all P<0.05), with an AUC of 0.876 (95%CI: 0.837-0.915) in the training dataset and 0.844 (95% CI: 0.801-0.887) in the validation dataset (Table 4 and Figure 3). Figure 4 displays color-coded feature maps of the identified texture features derived from ADC- and T2WI images for qualitative visualization of the features. This figure demonstrates distinctive textures between benign and malignant cases.

Discriminative performance and clinical usefulness of radiomic nomogram

Multivariate logistic regression analysis of PV, TZV, PSAD, TZ-PSAD, and fusion radscore demonstrated that only TZV (P=0.011) and fusion radscore (P<0.001) were identified as two independent risk factors of cancer. The radiomic nomogram was developed based on TZV and radscore (Figure 5), the formula was as follows: nomogram score = -1.749 -0.033*TZV + 5.825*radscore. The radiomic nomogram achieved an AUC of 0.905 (95%CI: 0.870-0.940) in the training dataset and 0.872

TABLE 2 Comparison of clinic-radiological characteristics between benign and malignant prostatic lesions.

	All (n=136)	Benign (n=87)	Malignant (n=49)	P-value
Age, years	67 (62, 73)	67 (62, 71)	67 (61.5, 75)	0.678
TPSA	7.6 (6.08, 9.32)	7.4 (6.2, 9.2)	8 (5.81,10)	0.818
FPSA	1.1 (0.7, 1.7)	1.14 (0.8,1.72)	0.93 (0.54,1.86)	0.230
FPSA/TPSA	0.15 (0.1, 0.23)	0.16 (0.12, 0.22)	0.13 (0.09, 0.26)	0.355
PV	52.71 (35.39, 73.58)	63.01 (42.83, 77.69)	35.02 (26.95, 55.74)	<0.001
TZV	27.11 (11.77, 41.79)	33.69 (18.48, 52.19)	13.89(7.38,29.5)	<0.001
PZV	24.11(17.17,32.72)	27.04 (18.23, 34.39)	21.64 (14.43, 30.33)	0.097
PSAD	0.14 (0.1, 0.19)	0.13 (0.1, 0.16)	0.19 (0.1, 0.28)	0.010
TZ-PSAD	0.27 (0.16, 0.53)	0.22 (0.15, 0.42)	0.36 (0.22, 0.94)	0.001
PZ-PSAD	0.30 (0.21, 0.44)	0.28 (0.21, 0.42)	0.36 (0.19, 0.46)	0.607
PI-RADS				>0.999
1	2 (1.5)	1 (1.1)	1 (2.0)	
2	44 (32.4)	28 (32.2)	16 (32.7)	
3	90 (66.2)	58 (66.7)	32 (65.3)	

Unless otherwise indicated, continuous variables were presented as median (interquartile range, IQR), and categorical variables were presented as number (%).
TPSA, total prostate specific antigen; FPSA, free prostate specific antigen; PV, prostate volume; TZV, transitional zone volume; PZV, peripheral zone volume; PSAD, prostate specific antigen density; TZ-PSAD, prostate transitional zone-specific antigen density; PZ-PSAD, prostate peripheral specific antigen density; PI-RADS, Prostate Imaging Reporting and Data System.

TABLE 3 Univariate and multivariate logistic regression analyses of risk factors for cancer.

Variables	Univariate analysis		Multivariate analysis	
	OR (95%CI)	p	OR (95%CI)	p
Age, years	1.01 (0.96-1.06)	0.790		
PI-RADS				
2	Ref			
3	1.19 (0.50-2.84)	0.697		
TPSA	0.91 (0.76-1.10)	0.345		
FPSA	0.97 (0.68-1.38)	0.865		
FPSA/TPSA	0.57 (0.02-14.75)	0.735		
PV	0.98 (0.97-1.00)	0.045		
TZV	0.97 (0.95-0.99)	0.009		
PZV	1.01 (0.97-1.04)	0.749		
PSAD	1504.68 (6.53-346905.17)	0.008		
TZ-PSAD	17.91 (3.45-93.00)	0.001	17.91 (3.45-93.00)	0.001
PZ-PSAD	0.74 (0.12-4.72)	0.746		

OR, odds ratio; PI-RADS, Prostate Imaging Reporting and Data System; TPSA, total prostate specific antigen; FPSA, free prostate specific antigen; PV, prostate volume; TZV, transitional zone volume; PZV, peripheral zone volume; PSAD, prostate specific antigen density; TZ-PSAD, prostate transitional zone-specific antigen density; PZ-PSAD, prostate peripheral specific antigen density.

(95%CI: 0.835-0.909) in the validation dataset, which was higher than TZ-PSAD and fusion radscore (all P values<0.05) (Table 4 and Figure 3). The calibration curves of the radiomic nomogram demonstrated accepted agreement between prediction and actual observation (Figure 5), as verified by Hosmer-Lemeshow tests (training dataset: P=0.234; validation dataset: P=0.172). The DCA and CIC showed the clinical usefulness of the risk prediction nomogram.

Discussion

This present study demonstrated that the radiomic model based on bpMRI achieved good performance in capturing the heterogeneity of prostatic diseases, which could be used to distinguish PCa from hyperplasia in a non-invasive way. The PSA-based screening strategy is not actable in patients with PI-RADS ≤3 lesions and PSA level of 4-10 ng/mL. However, the

TABLE 4 The performance comparison of various models.

Dataset	Models	AUC (95%CI)	P	Sensitivity (%)	Specificity (%)	Accuracy
Training cohort	TZ-PSAD	0.712 (0.655-0.769)	<0.001	67.6	65.6	66.3
	ADC-based radscore	0.743 (0.690-0.796)	<0.001	64.7	68.9	67.4
	T2WI-based radscore	0.816 (0.765-0.867)	<0.001	82.4	73.8	76.8
	Fusion radscore	0.876 (0.837-0.915)	Ref.	85.3	73.8	77.9
	Radiomic nomogram	0.905 (0.870-0.940)	<0.001	88.2	85.2	86.3
Validation cohort	TZ-PSAD	0.592 (0.527-0.657)	<0.001	60.0	53.8	56.1
	ADC-based radscore	0.779 (0.730-0.828)	0.038	73.3	65.4	68.3
	T2WI-based radscore	0.808 (0.761-0.855)	<0.001	73.3	76.9	75.6
	Fusion radscore	0.844 (0.801-0.887)	Ref.	80.0	84.6	82.9
	Radiomic nomogram	0.872 (0.835-0.909)	0.002	73.3	84.6	80.5

AUC, area under the curve; TZ-PSAD, prostate transitional zone-specific antigen density; ADC, apparent-diffusion coefficient; T2WI, T2-weighted imaging.

TABLE 5 Radiomic features contained in the ADC-based and T2WI-based radiomic models.

ADC

original_glszm_ZoneEntropy

log-sigma-5-0-mm-3D_firstorder_Range

log-sigma-5-0-mm-3D_glszm_ZoneEntropy

wavelet-HLH_glszm_GrayLevelNonUniformityNormalized

wavelet-LLL_glrlm_LongRunLowGrayLevelEmphasis

wavelet-LLL_glszm_SizeZoneNonUniformity

T2WI

log-sigma-1-0-mm-3D_firstorder_Kurtosis

log-sigma-5-0-mm-3D_glszm_SmallAreaEmphasis

log-sigma-5-0-mm-3D_glszm_SmallAreaHighGrayLevelEmphasis

wavelet-LLH_firstorder_Maximum

wavelet-LLH_glcm_ClusterShade

wavelet-LHH_gldm_HighGrayLevelEmphasis

wavelet-HLL_firstorder_Variance

wavelet-HLH_firstorder_Entropy

wavelet-HLH_glszm_GrayLevelNonUniformityNormalized

wavelet-HHL_firstorder_Skewness

wavelet-HHH_gldm_HighGrayLevelEmphasis

wavelet-LLL_firstorder_Minimum

wavelet-LLL_ngtdm_Busyness

ADC, apparent-diffusion coefficient; T2WI, T2-weighted imaging.

radiomic nomogram combining TZV and fusion radscore can individually predict the probability of PCa with high accuracy and good calibration and clinical utility.

In recent years, mpMRI has been increasingly applied for the qualitative evaluation of PCa (26, 27). The PI-RADS was proposed for better standardization of prostate MRI performance and image interpretation. PI-RADS v 2.1 in 2019 introduced the concept of bpMRI (T2WI and DWI) to simplify prostate MRI (20). Prostate MRI categorizes suspected PCa into low- and high-risk, with risk scores ranging from 1 to 5. PI-RADS hinges on the subjective judgment of radiologists, which is prone to inter-reader variability (28). A recent meta-analysis (29) showed varied inter-reader agreements of PI-RADS v2.1 and moderate inter-reader reliability (pooled k value of 0.65) among radiologists for whole gland and TZ lesions. Nonetheless, PI-RAS 2.1 has higher inter-reader reproducibility than version 2.0 (30). One of the most crucial challenges for clinicians is the occurrence of equivocal or PI-RADS 3 findings (31). While biopsy is recommended for PI-RADS 4 or 5 lesions, PI-RADS 3 lesions are considered borderline results with no definite recommendation or conclusion (20). Although PI-RADS 1 or 2 are not recommended for undergoing an imaging-guided biopsy, such an approach may miss a small portion of PCa due to the low cancer detection rate for PI-RADS 1 (6%; range, 0-20%) and PI-RADS 2 (9%; range, 5-13%) in the patient-level analysis (32). Additionally, whether patients with a serum PSA level of 4-10 ng/mL should be recommended for a biopsy is

clinically challenging (33). In this current study, we focused on patients with both PI-RADS ≤3 lesions and PSA level of 4-10 ng/mL, which has not yet been reported in previous literature.

The clinical application of PSA has several limitations, leading to overdiagnosis and overtreatment (34, 35). Therefore, new methods for accurate risk stratification of prostatic nodules and reducing unnecessary biopsies are desirable to improve the management of PCa and patient prognosis. In recent years, non-invasive, cost-effective, high-accuracy liquid biopsy biomarkers such as DNA methylation have been developed for early diagnosis of PCa (36). However, liquid biopsy biomarkers still lack large-scale validation and have methodological and biological limitations, precluding implementation in clinical practice. Radiomics refers to the high-throughput mining of quantitative image features from standard-of-care medical images that enables to uncover of disease characteristics including biological property and tumor heterogeneity that fail to be appreciated by the naked eye (37). Radiomics provides a non-invasive way to evaluate PCa better than morphological visual interpretation. Li et al. (11) constructed a radiomic model based on mpMRI including T2WI, ADC, DWI, and DCE imaging and achieved an AUC of 0.86 when tested, improving diagnostic performance of PI-RADS v2.1 in PI-RADS categories 1-5 PCa. Qi et al. (33) found that mpMRI radiomics outperformed single sequence-based models; however, they did not explore the added value of DCE to T2WI and ADC. The results showed that the AUC of DCE model was lower than that of ADC and T2WI models (0.774 vs 0.853 vs 0.828). Thus, it seems that DCE may be difficult to bring significantly incremental value to bpMRI. Jing et al. (9) compared the combination of lesion segmentation and whole prostate segmentation on T2WI and DWI to establish the optimal radiomic methodology. The results showed that the radiomic model based on whole prostate T2WI and lesion DWI achieved the best performance in predicting clinically significant PCa, which was superior to PI-RADS scores (9). However, Montoya et al. (38) showed that bpMRI radiomics and kallikreins failed to outperform PI-RADS v2.1 scores and their combination did not achieve further performance improvement. Some studies compared different classifiers in the prospective diagnosis of prostate diseases based on mpMRI and found that the RF classifier performed better than other classifiers (39–42). Gui et al. (43) built a radiomic nomogram combing T2WI-based radiomic features and PSA yielded an AUC of 0.90 in the differential diagnosis of PCa and hyperplasia. Given that various deep-learning- and radiomics-based methods have been proposed for PCa classification, Castillo T et al. (44) compared the value of a deep-learning model with that of a radiomic model for the PCa diagnosis and concluded that the radiomic model was more accurate than a fully automated deep-learning model (AUC: 0.65-0.88 vs 0.44-0.73). Zhang et al. (45) showed that perilesional radiomic features could enhance the discrimination ability of the
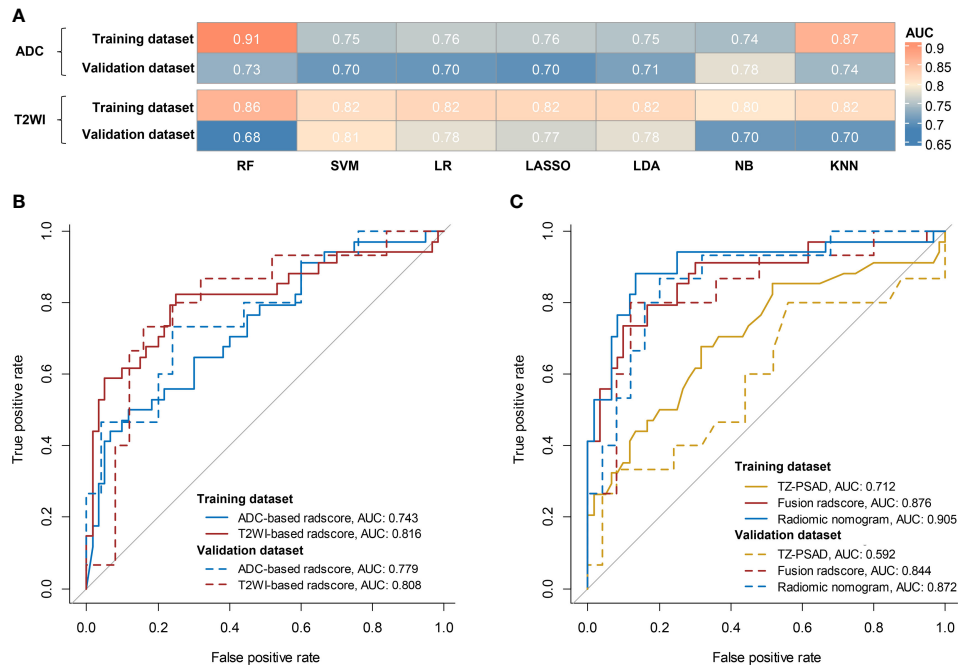
FIGURE 3
Diagnostic performance of models. **(A)** comparison of AUCs of different classifiers for ADC and T2WI, respectively; **(B)** ROC of the optimal single-layered radscore; **(C)** ROC of TZV, fusion radscore, and radiomic nomogram.
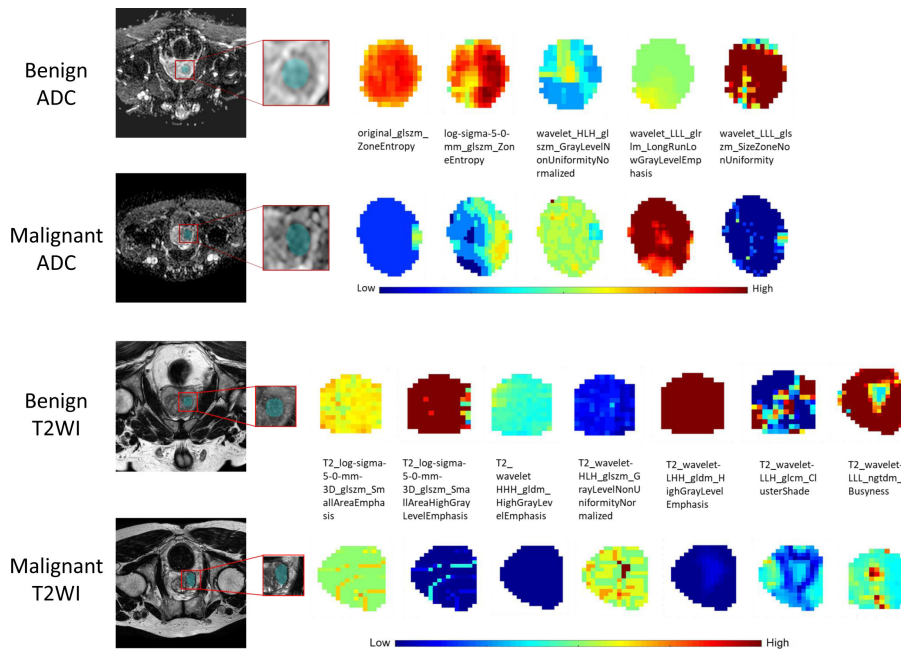
FIGURE 4
The visual feature maps of the selected texture features extracted from ADC- and T2WI images of benign and malignant cases.
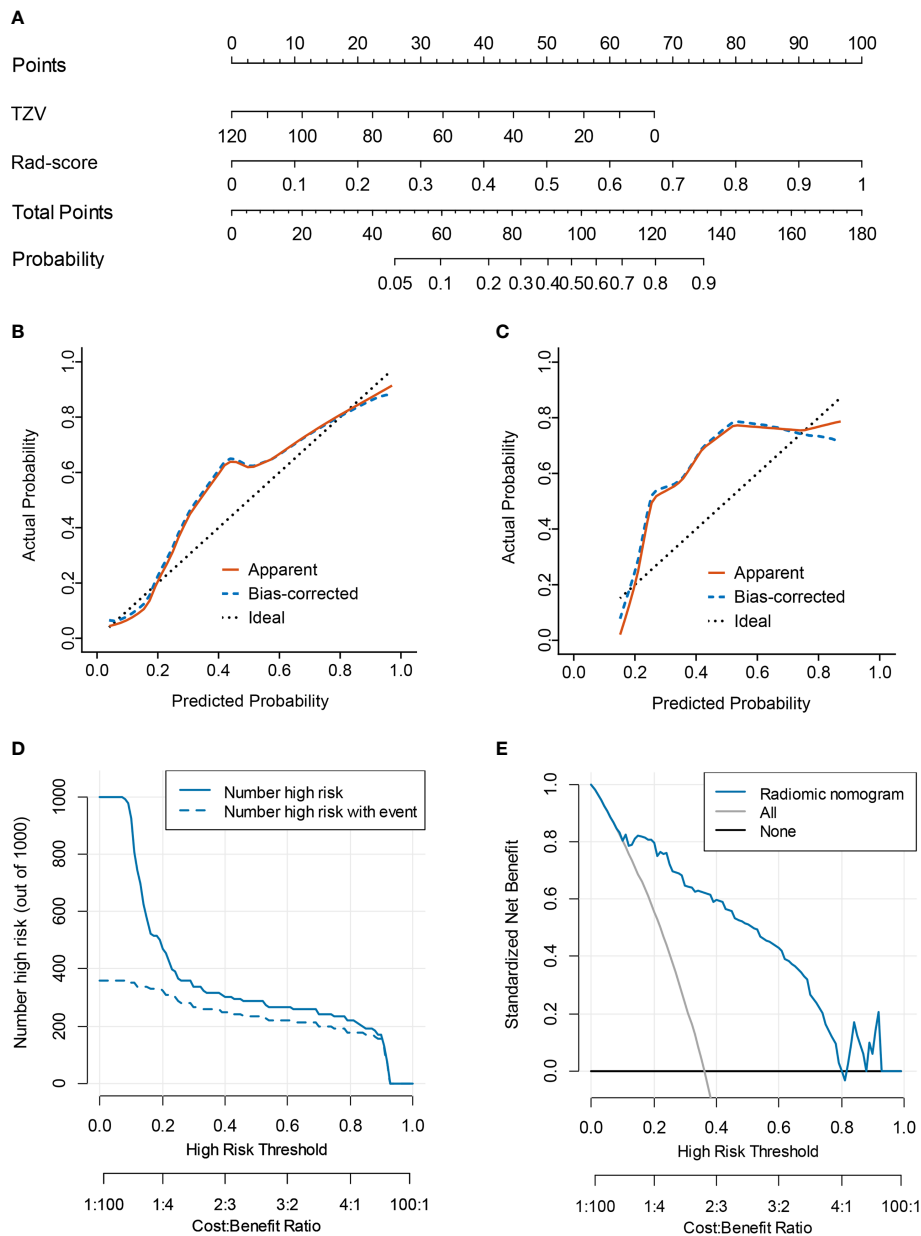
FIGURE 5
Nomogram performance for predicting probability of PCa. **(A)** nomogram; **(B)** calibration curve of training dataset; **(C)** calibration curve of validation dataset; **(D)** clinical decision curve; **(E)** clinical impact curve.

intralesional radiomic features. Lim et al. (46) indicated a moderate accuracy for T2WI (0.547) and ADC (0.684) for determining which PI-RADS category 3 lesions represent PCa. Considering the performance of radiomic model depends on feature selection and the employed machine learning algorithms, in this study, we carried out rigorous feature selection and compared seven machine learning classifiers to find the most suitable methods to build radiomic models, with an AUC of 0.84 in the validation dataset.

This study also has several limitations. First, this is a retrospective study performed in a single center with a relatively small sample size, which may indicate selection bias and low generalizability of the findings. Therefore, larger multicenter studies are warranted for reducing the effects of selection bias on model accuracy. Second, this study used manual segmentation rather than semi-automatic or automatic delineation, which was labored and time-consuming. Third, this study was unable to test a more advanced approach such as

deep-learning for the prediction of PCa in such a population, which may show more merits and deserve further investigation. Finally, biological interpretability of texture features is lacking. Efforts to introduce biological meaning into radiomics are gaining traction in this field with distinct emerging approaches available, such as correlation with pathology features and biological function, radiology–pathology coregistration, and analysis of biological pathways or genomic correlations in humans or animals ([47]).

Conclusion

In this study, we investigated the role of radiomic features derived from bpMRI (T2WI plus ADC) in the differentiation of PCa and hyperplasia. The combination of T2WI and ADC was superior to a single sequence in predicting PCa. The radiomic nomogram integrating TZV and radscore has the potential to accurate and noninvasive identification of PCa in patients with PI-RADS ≤3 lesions and PSA of 4-10 ng/mL, which could reduce unnecessary biopsy.

In the future, liquid biopsy diagnostic biomarkers can be added to improve the performance of MRI in early screening of PCa.

Data availability statement

The raw data supporting the conclusions of this article will be made available by the authors, without undue reservation.

Ethics statement

The studies involving human participants were reviewed and approved by Zhongshan City People's Hospital. The ethics committee waived the requirement of written informed consent for participation.

Author contributions

YBL and YXZ designed the study, collected and analyzed data, obtained the grant, wrote the manuscript; HXH, FBL, RQY assisted with data analysis and manuscript preparation. QL, QW, RZ, YQH, and CYL assisted with subject recruitment, data collection and analysis, manuscript review. All authors contributed to the article and approved the submitted version.

Funding

Conflict of interest

The authors declare that the research was conducted in the absence of any commercial or financial relationships that could be construed as a potential conflict of interest.

Publisher's note

All claims expressed in this article are solely those of the authors and do not necessarily represent those of their affiliated organizations, or those of the publisher, the editors and the reviewers. Any product that may be evaluated in this article, or claim that may be made by its manufacturer, is not guaranteed or endorsed by the publisher.

References

1. Sung H, Ferlay J, Siegel RL, Laversanne M, Soerjomataram I, Jemal A, et al. Global cancer statistics 2020: GLOBOCAN estimates of incidence and mortality worldwide for 36 cancers in 185 countries. *CA Cancer J Clin* (2021) 71:209–49. doi: 10.3322/caac.21660

2. Turkbey B, Brown AM, Sankineni S, Wood BJ, Pinto PA, Choyke PL. Multiparametric prostate magnetic resonance imaging in the evaluation of prostate cancer. *CA Cancer J Clin* (2016) 66:326–36. doi: 10.3322/caac.21333

3. Johnson LM, Turkbey B, Figg WD, Choyke PL. Multiparametric MRI in prostate cancer management. *Nat Rev Clin Oncol* (2014) 11:346–53. doi: 10.1038/nrclinonc.2014.69

4. Dwivedi DK, Jagannathan NR. Emerging MR methods for improved diagnosis of prostate cancer by multiparametric MRI. *MAGMA* (2022) 35:587–608. doi: 10.1007/s10334-022-01031-5

5. Castro HAS, Iared W, Santos JEM, Solha RS, Shigueoka DC, Ajzen SA. Impact of PSA density of transition zone as a potential parameter in reducing the number of unnecessary prostate biopsies in patients with psa levels between 2. 6 10.0 ng/mL *Int Braz J Urol* (2018) 44:709–16. doi: 10.1590/s1677-5538.ibju.2017.0506

6. Sathianathen NJ, Omer A, Harriss E, Davies L, Kasivisvanathan V, Punwani S, et al. Negative predictive value of multiparametric magnetic resonance imaging in the detection of clinically significant prostate cancer in the prostate imaging reporting and data system era: A systematic review and meta-analysis. *Eur Urol* (2020) 78:402–14. doi: 10.1016/j.eururo.2020.03.048

7. Stabile A, Giganti F, Rosenkrantz AB, Taneja SS, Villeirs G, Gill IS, et al. Multiparametric MRI for prostate cancer diagnosis: current status and future directions. *Nat Rev Urol* (2020) 17:41–61. doi: 10.1038/s41585-019-0212-4

8. Lambin P, Leijenaar RTH, Deist TM, Peerlings J, de Jong EEC, van Timmeren J, et al. Radiomics: the bridge between medical imaging and personalized medicine. *Nat Rev Clin Oncol* (2017) 14:749–62. doi: 10.1038/nrclinonc.2017.141

9. Jing G, Xing P, Li Z, Ma X, Lu H, Shao C, et al. Prediction of clinically significant prostate cancer with a multimodal MRI-based radiomics nomogram. *Front Oncol* (2022) 12:918830. doi: 10.3389/fonc.2022.918830

10. Cheng X, Chen Y, Xu H, Ye L, Tong S, Li H, et al. Avoiding unnecessary systematic biopsy in clinically significant prostate cancer: Comparison between MRI-based radiomics model and PI-RADS category. *J Magn Reson Imaging* (2022). doi: 10.1002/jmri.28333

11. Li M, Yang L, Yue Y, Xu J, Huang C, Song B. Use of radiomics to improve diagnostic performance of PI-RADS v2. *1 Prostate Cancer Front Oncol* (2020) 10:631831. doi: 10.3389/fonc.2020.631831

12. Woźnicki P, Westhoff N, Huber T, Riffel P, Froelich MF, Gresser E, et al. Multiparametric MRI for prostate cancer characterization: Combined use of radiomics model with PI-RADS and clinical parameters. *Cancers (Basel)* (2020) 12(7):1767. doi: 10.3390/cancers12071767

13. Wang J, Wu CJ, Bao ML, Zhang J, Wang XN, Zhang YD, et al. Machine learning-based analysis of MR radiomics can help to improve the diagnostic performance of PI-RADS v2 in clinically relevant prostate cancer. *Eur Radiol* (2017) 27:4082–90. doi: 10.1007/s00330-017-4800-5

14. Weinreb JC, Barentsz JO, Choyke PL, Cornud F, Haider MA, Macura KJ, et al. PI-RADS prostate imaging - reporting and data system: 2015, version 2. *Eur Urol* (2016) 69:16–40. doi: 10.1016/j.eururo.2015.08.052

15. Drost FH, Osses DF, Nieboer D, Steyerberg EW, Bangma CH, Roobol MJ, et al. Prostate MRI, with or without MRI-targeted biopsy, and systematic biopsy for detecting prostate cancer. *Cochrane Database Syst Rev* (2019) 4:CD012663. doi: 10.1002/14651858.CD012663.pub2

16. Niaf E, Lartizien C, Bratan F, Roche L, Rabilloud M, Mège-Lechevallier F, et al. Prostate focal peripheral zone lesions: characterization at multiparametric MR imaging– influence of a computer-aided diagnosis system. *Radiology* (2014) 271:761–9. doi: 10.1148/radiol.14130448

17. Deng L, Wang QP, Chen X, Duan XY, Wang W, Guo YM. The combination of diffusion- and T2-weighted imaging in predicting deep myometrial invasion of endometrial cancer: A systematic review and meta-analysis. *J Comput Assist Tomogr* (2015) 39:661–73. doi: 10.1097/RCT.0000000000000280

18. De Visschere P, Lumen N, Ost P, Decaestecker K, Pattyn E, Villeirs G. Dynamic contrast-enhanced imaging has limited added value over T2-weighted imaging and diffusion-weighted imaging when using PI-RADSv2 for diagnosis of clinically significant prostate cancer in patients with elevated PSA. *Clin Radiol* (2017) 72:23–32. doi: 10.1016/j.crad.2016.09.011

19. Ma XZ, Lv K, Sheng JL, Yu YX, Pang PP, Xu MS, et al. Application evaluation of DCE-MRI combined with quantitative analysis of DWI for the diagnosis of prostate cancer. *Oncol Lett* (2019) 17:3077–84. doi: 10.3892/ol.2019.9988

20. Turkbey B, Rosenkrantz AB, Haider MA, Padhani AR, Villeirs G, Macura KJ, et al. Prostate imaging reporting and data system version 2.1: 2019 update of prostate imaging reporting and data system version 2. *Eur Urol* (2019) 76:340–51. doi: 10.1016/j.eururo.2019.02.033

21. Greenberg JW, Koller CR, Casado C, Triche BL, Krane LS. A narrative review of biparametric MRI (bpMRI) implementation on screening, detection, and the overall accuracy for prostate cancer. *Ther Adv Urol* (2022) 14:17562872221096377. doi: 10.1177/17562872221096377

22. Han C, Liu S, Qin XB, Ma S, Zhu LN, Wang XY. MRI Combined with PSA density in detecting clinically significant prostate cancer in patients with PSA serum levels of 4~10 ng/mL: Biparametric versus multiparametric MRI. *Diagn Interv Imaging* (2020) 101:235–44. doi: 10.1016/j.diii.2020.01.014

23. Wallström J, Geterud K, Kohestani K, Maier SE, Månsson M, Pihl CG, et al. Bi- or multiparametric MRI in a sequential screening program for prostate cancer with PSA followed by MRI? results from the göteborg prostate cancer screening 2 trial. *Eur Radiol* (2021) 31:8692–702. doi: 10.1007/s00330-021-07907-9

24. Zwanenburg A, Vallières M, Abdalah MA, Aerts HJWL, Andrearczyk V, Apte A, et al. The image biomarker standardization initiative: Standardized quantitative radiomics for high-throughput image-based phenotyping. *Radiology* (2020) 295:328–38. doi: 10.1148/radiol.2020191145

25. van Griethuysen JJM, Fedorov A, Parmar C, Hosny A, Aucoin N, Narayan V, et al. Computational radiomics system to decode the radiographic phenotype. *Cancer Res* (2017) 77:e104–7. doi: 10.1158/0008-5472.CAN-17-0339

26. Ueno Y, Tamada T, Bist V, Reinhold C, Miyake H, Tanaka U, et al. Multiparametric magnetic resonance imaging: Current role in prostate cancer management. *Int J Urol* (2016) 23:550–7. doi: 10.1111/iju.13119

27. Aydın H, Kızılgöz V, Tekin BO. Overview of current multiparametric magnetic resonance imaging approach in the diagnosis and staging of prostate cancer. *Kaohsiung J Med Sci* (2015) 31:167–78. doi: 10.1016/j.kjms.2015.01.002

28. Muller BG, Shih JH, Sankineni S, Marko J, Rais-Bahrami S, George AK, et al. Prostate cancer: Interobserver agreement and accuracy with the revised prostate imaging reporting and data system at multiparametric MR imaging. *Radiology* (2015) 277:741–50. doi: 10.1148/radiol.2015142818

29. Wen J, Ji Y, Han J, Shen X, Qiu Y. Inter-reader agreement of the prostate imaging reporting and data system version v2.1 for detection of prostate cancer: A systematic review and meta-analysis. *Front Oncol* (2022) 12:1013941. doi: 10.3389/fonc.2022.1013941

30. Zhao J, Mangarova DB, Brangsch J, Kader A, Hamm B, Brenner W, et al. Correlation between intraprostatic PSMA uptake and MRI PI-RADS of [68Ga]Ga-PSMA-11 PET/MRI in patients with prostate cancer: Comparison of PI-RADS version 2.0 and PI-RADS version 2.1. *Cancers (Basel)* (2020) 12:3523. doi: 10.3390/cancers12123523

31. Ullrich T, Quentin M, Arsov C, Schmaltz AK, Tschischka A, Laqua N, et al. Risk stratification of equivocal lesions on multiparametric magnetic resonance imaging of the prostate. *J Urol* (2018) 199:691–8. doi: 10.1016/j.juro.2017.09.074

32. Schoots IG, Padhani AR, Rouvière O, Barentsz JO, Richenberg J. Analysis of magnetic resonance imaging-directed biopsy strategies for changing the paradigm of prostate cancer diagnosis. *Eur Urol Oncol* (2020) 3:32–41. doi: 10.1016/j.euo.2019.10.001

33. Qi Y, Zhang S, Wei J, Zhang G, Lei J, Yan W, et al. Multiparametric MRI-based radiomics for prostate cancer screening with PSA in 4-10 ng/mL to reduce unnecessary biopsies. *J Magn Reson Imaging* (2020) 51:1890–9. doi: 10.1002/jmri.27008

34. Salami SS, Vira MA, Turkbey B, Fakhoury M, Yaskiv O, Villani R, et al. Multiparametric magnetic resonance imaging outperforms the prostate cancer prevention trial risk calculator in predicting clinically significant prostate cancer. *Cancer* (2014) 120:2876–82. doi: 10.1002/cncr.28790

35. Bhat NR, Vetter JM, Andriole GL, Shetty AS, Ippolito JE, Kim EH. Magnetic resonance imaging-defined prostate-specific antigen density significantly improves the risk prediction for clinically significant prostate cancer on biopsy. *Urology* (2019) 126:152–7. doi: 10.1016/j.urology.2018.12.010

36. Matuszczak M, Schalken JA, Salagierski M. Prostate cancer liquid biopsy biomarkers' clinical utility in diagnosis and prognosis. *Cancers (Basel)* (2021) 13 (13):3373. doi: 10.3390/cancers13133373

37. Gillies RJ, Kinahan PE, Hricak H. Radiomics: Images are more than pictures, they are data. *Radiology* (2016) 278:563–77. doi: 10.1148/radiol.2015151169

38. Montoya Perez I, Merisaari H, Jambor I, Ettala O, Taimen P, Knaapila J, et al. Detection of prostate cancer using biparametric prostate MRI, radiomics, and kallikreins: A retrospective multicenter study of men with a clinical suspicion of prostate cancer. *J Magn Reson Imaging* (2022) 55:465–77. doi: 10.1002/jmri.27811

39. Li L, Gu L, Kang B, Yang J, Wu Y, Liu H, et al. Evaluation of the efficiency of MRI-based radiomics classifiers in the diagnosis of prostate lesions. *Front Oncol* (2022) 12:934108. doi: 10.3389/fonc.2022.934108

40. Peng T, Xiao J, Li L, Pu B, Niu X, Zeng X, et al. Can machine learning-based analysis of multiparameter MRI and clinical parameters improve the performance of clinically significant prostate cancer diagnosis? *Int J Comput Assist Radiol Surg* (2021) 16:2235–49. doi: 10.1007/s11548-021-02507-w

41. Ji X, Zhang J, Shi W, He D, Bao J, Wei X, et al. Bi-parametric magnetic resonance imaging based radiomics for the identification of benign and malignant prostate lesions: cross-vendor validation. *Phys Eng Sci Med* (2021) 44:745–54. doi: 10.1007/s13246-021-01022-1

42. Hectors SJ, Chen C, Chen J, Wang J, Gordon S, Yu M, et al. Magnetic resonance imaging radiomics-based machine learning prediction of clinically significant prostate cancer in equivocal PI-RADS 3 lesions. *J Magn Reson Imaging* (2021) 54:1466–73. doi: 10.1002/jmri.27692

43. Gui S, Lan M, Wang C, Nie S, Fan B. Application value of radiomic nomogram in the differential diagnosis of prostate cancer and hyperplasia. *Front Oncol* (2022) 12:859625. doi: 10.3389/fonc.2022.859625

44. Castillo TJM, Arif M, Starmans MPA, Niessen WJ, Bangma CH, Schoots IG, et al. Classification of clinically significant prostate cancer on multi-parametric MRI: A validation study comparing deep learning and radiomics. *Cancers (Basel)* (2021) 14(1):12. doi: 10.3390/cancers14010012

45. Zhang H, Li X, Zhang Y, Huang C, Wang Y, Yang P, et al. Diagnostic nomogram based on intralesional and perilesional radiomics features and clinical factors of clinically significant prostate cancer. *J Magn Reson Imaging* (2021) 53:1550–8. doi: 10.1002/jmri.27486

46. Lim CS, Abreu-Gomez J, Thornhill R, James N, Al Kindi A, Lim AS, et al. Utility of machine learning of apparent diffusion coefficient (ADC) and T2-weighted (T2W) radiomic features in PI-RADS version 2.1 category 3 lesions to predict prostate cancer diagnosis. *Abdom Radiol (NY)* (2021) 46:5647–58. doi: 10.1007/s00261-021-03235-0

47. Tomaszewski MR, Gillies RJ. The biological meaning of radiomic features. *Radiology* (2021) 298:505–16. doi: 10.1148/radiol.2021202553